

On-demand indistinguishable single photons from an efficient and pure source based on a Rydberg ensemble

D.P. Ornelas-Huerta,¹ A.N. Craddock,¹ E.A. Goldschmidt,^{2,3} A.J. Hachtel,¹
Y. Wang,¹ P. Bienias,^{1,4} A.V. Gorshkov,^{1,4} S.L. Rolston,¹ and J.V. Porto¹

¹*Joint Quantum Institute, NIST/University of Maryland, College Park, MD 20742, USA*

²*Department of Physics, University of Illinois at Urbana-Champaign,
1110 W. Green Street, Urbana, Illinois 61801, USA*

³*US Army Research Laboratory, Adelphi, Maryland 20783, USA*

⁴*Joint Center for Quantum Information and Computer Science,
NIST/University of Maryland, College Park, MD 20742, USA*

Single photons coupled to atomic systems have shown to be a promising platform for developing quantum technologies. Yet a bright on-demand, highly pure and highly indistinguishable single-photon source compatible with atomic platforms is lacking. In this work, we demonstrate such a source based on a strongly interacting Rydberg system. The large optical nonlinearities in a blockaded Rydberg ensemble convert coherent light into a single-collective excitation that can be coherently retrieved as a quantum field. We observe a single-transverse-mode efficiency up to 0.18(2), $g^{(2)} = 2.0(1.5) \times 10^{-4}$, and indistinguishability of 0.982(7), making this system promising for scalable quantum information applications. Accounting for losses, we infer a generation probability up to 0.40(4). Furthermore, we investigate the effects of contaminant Rydberg excitations on the source efficiency. Finally, we introduce metrics to benchmark the performance of on-demand single-photon sources.

INTRODUCTION

Engineering single-photon sources with high efficiency, purity, and indistinguishability is a longstanding goal for applications such as linear optical quantum computation [1], boson sampling [2], quantum networks [3] and quantum metrology [4]. Atomic systems have shown significant progress towards quantum light-matter interfaces, including efficient quantum memories [5], quantum networks [6], high-fidelity light-matter entanglement [7], atomic gates [8], and quantum simulators [9]. Atomic platforms require spectrally matched single photons that can coherently couple with atomic processors, provided with high-efficiency generation, purity, and indistinguishability.

Strongly interacting Rydberg atoms provide a particularly promising system. They have proven to be versatile for engineering strong interactions between photons, exhibiting nonlinearities at the single-photon level [10–13]. Recent experiments using Rydberg interactions have demonstrated on-demand single-photon generation [14, 15], as well as photon transistors [16–18], photonic and atomic phase gates [19–24], high-visibility quantum interference in hybrid systems [25], and quantum simulators [26–29].

We describe here an efficient single-photon source based on collective excitation and de-excitation of a cold, trapped ensemble of atoms through a highly excited Rydberg state [14, 15, 30]. During two-photon excitation from the ground to the Rydberg state via an intermediate state [see Fig. 1(a)], long-range van der Waals interactions suppress multiple Rydberg excitations within a blockade radius, r_b [31]. The resulting single, col-

lective atomic excitation is coherently shared among N atoms as a spin wave [30]. Due to the collective nature of the excitation, if the initial phase coherence of the spin wave is maintained, the subsequent coupling of the Rydberg state to the intermediate state can efficiently map the excitation onto a single photon in a well-defined mode [32]. Our system produces single photons with repetition rates up to 400 kHz, a generation probability up to 0.40(4), $g^{(2)} = 2.0(1.5) \times 10^{-4}$, and indistinguishability of 0.982(7). We model the write and retrieval process, including the measured spin-wave dephasing rate. We identify long-lived-contaminant Rydberg states [33] as a limiting factor on the source efficiency for increasing production rates.

Given the requirements for most quantum information applications, the single-mode efficiency, rate, and quality of single-photon sources are of key importance since successful scaling of these systems involves detection of multiple identical photons. Thus, we introduce metrics to describe the probability, rate, and fidelity of producing a single photon in a single-mode, which includes the contributions from the commonly used metrics: overall collection efficiency, purity, indistinguishability, and repetition rate [34].

EXPERIMENTAL APPARATUS AND PROCEDURE

We start the experiment with a magneto-optical trap of ^{87}Rb atoms and further laser cool the atoms with a Λ -gray molasses down to $\approx 10 \mu\text{K}$. We load the atoms into a 1003-nm wavelength optical dipole trap. To write the

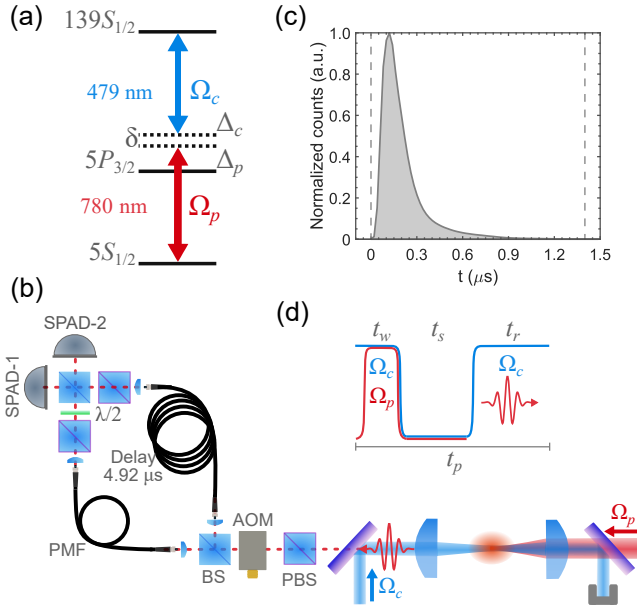


FIG. 1. (a) Relevant atomic levels and set-up for single-photon generation. During the spin wave writing stage we set the single-photon detuning $\Delta_p \approx 2\pi \times 50$ MHz, and the two-photon detuning $\delta = \Delta_p + \Delta_c$ to Raman resonance, $\delta \approx -2\pi \times 2$ MHz. For retrieval, $\Delta_c \approx 2\pi \times 7$ MHz. (b) Experimental set-up schematic. There is a polarization beamsplitter (PBS) to project the photons into a single polarization mode, followed by an acousto-optic-modulator (AOM) that gates the incoming photons. All the light is directed to the polarization maintaining fiber (PMF) to realize a purity measurement. For the indistinguishability characterization, we split the light such that the rate is roughly the same at both ports of the second beamsplitter (BS). By rotating the half waveplate ($\lambda/2$) we can control the relative polarization of the photons coming from the PMF port and the long delay port. (c) Photon temporal envelope, gray dashed lines indicate the software gate window. (d) Timing sequence for the generation of successive single photons, the writing π -pulse lasts for $t_w \approx 370$ ns. We use a minimum storage time $t_s \approx 350$ ns to maximize the retrieval and vary t_r to change the repetition rate, $R = 1/t_p$.

spin wave, we couple the ground state, $|g\rangle = |5S_{1/2}, F = 2, m_F = 2\rangle$ to the Rydberg state $|r\rangle = |139S_{1/2}, m_J = 1/2\rangle$ via the intermediate state $|e\rangle = |5P_{3/2}, F = 3, m_F = 3\rangle$ with an intermediate detuning $\Delta_p \approx 2\pi \times 50$ MHz, as shown in Figure 1(a). The probe beam coupling $|g\rangle$ to $|e\rangle$ is focused into the atom cloud with a waist of $\approx 3.3 \mu\text{m}$, with a Rabi frequency $\Omega_p \approx 2\pi \times 1$ MHz. The counter-propagating control beam coupling $|e\rangle$ to $|r\rangle$ has a larger, $\approx 19 \mu\text{m}$ waist and peak Rabi frequency $\Omega_c \approx 2\pi \times 7$ MHz.

The van der Waals coefficient of the Rydberg state $139S_{1/2}$ is $C_6 \approx -2\pi \times 2.5 \times 10^6$ GHz μm^6 [35], which results in a blockade radius $r_b \approx 60 \mu\text{m}$ during the spin-wave writing. Since r_b is larger than the probe beam waist and the atomic cloud extension in the propaga-

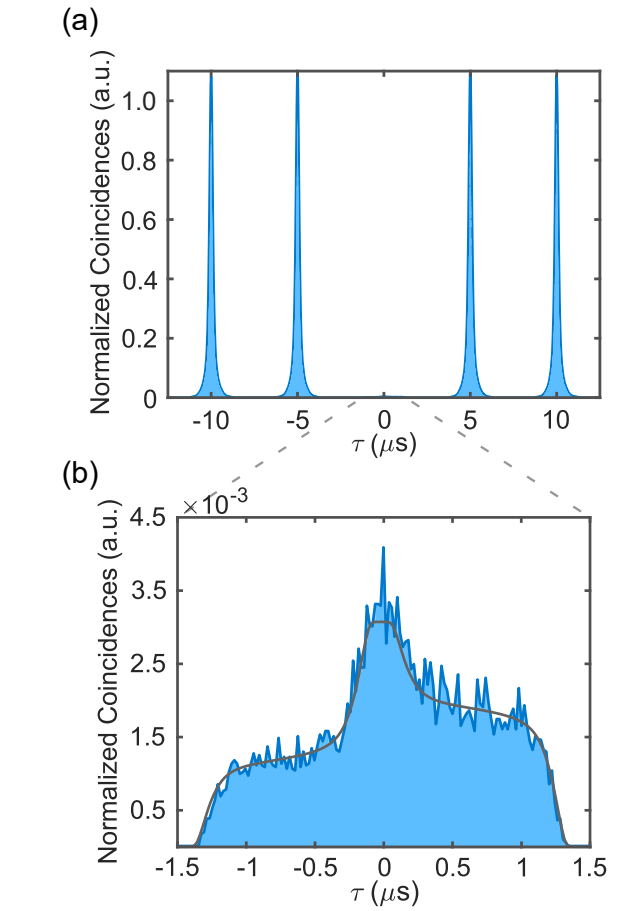


FIG. 2. Measured coincidences for purity and characterization. (a) Normalized coincidences for $g^{(2)}(\tau)$ with $5 \mu\text{s}$ cycle. (b) Normalized coincidences for $g^{(2)}(\tau)$ around $\tau = 0$, grey line represents the background coincidences with 20-ns bins. The shape of this profile arises from the convolution of the photon pulse shape with a constant background within the gate window, and the pedestal asymmetry is because the background rate is not the same for each channel. All data shown were taken with 60% duty cycle.

tion direction, $\sigma_z \approx 27 \mu\text{m}$, the excitation volume is blockaded. The effective two-photon Rabi frequency, $\Omega_{2\text{ph}} = \frac{\Omega_p \Omega_c}{2\Delta_p}$ is enhanced by a factor $\sqrt{N} \approx 20$ from the N atoms participating in the collective excitation [30, 36].

After a spin-wave storage time $t_s > 350$ ns [see Fig. 1(d)], we turn back on the control field with a detuning $\Delta_c \approx 2\pi \times 7$ MHz that maximizes the retrieval efficiency of the spin wave into a single photon. We can vary the repetition rate of the write-retrieval sequence up to 400 kHz, with interrogation times up to 600 ms (0.6 duty cycle) before we need to reload the optical dipole trap.

SINGLE-PHOTON SOURCE PURITY AND INDISTINGUISHABILITY

We use Hanbury Brown-Twiss and Hong-Ou-Mandel interferometers to characterize the purity and indistinguishability of our single photons [see Fig. 1(b)]. We define the purity of our single-photon source as $1 - g^{(2)}(0)$, where $g^{(2)}(\tau)$ is the second-order autocorrelation function. We apply a $1.4 \mu\text{s}$ long software gate window, containing more than 99.9% of the pulse [see Fig. 1(c)]. Coincidences at zero time delay are substantially suppressed, as shown in Figure 2(a), with strong antibunching $g_{\text{raw}}^{(2)}(0) = 0.0145(2)$, integrating the area around $\tau = 0$ and without background subtraction. The background coincidence rate is dominated by coincidences involving photon events with background counts unrelated to the single-photon generation, coming from detector dark counts and room light leakage. The independently measured background rate, photon shape, and photon rate are constant throughout each experimental run, from which we determine that the accidental coincidences contribute to $g_{\text{back}}^{(2)}(0) = 0.0143$. The gray curve in Figure 2(b) shows the background coincidence profile within the gate window (see [37] for details). After background subtraction, our single-photon source has $g^{(2)}(0) = 2.0(1.5) \times 10^{-4}$.

We use a Hong-Ou-Mandel interferometer (HOM) to measure the photon indistinguishability. We implement a fiber-based $4.92 \mu\text{s}$ delay in one arm to temporally overlap adjacently produced photons. Additionally, there is a polarizing beam splitter (PBS) at the output of each fiber to account for any polarization rotation due to the fibers. At the exit of the short arm, there is a half-wave plate (HWP) to rotate the polarization and control the degree of distinguishability of the photons. Figure 3(a) shows the normalized coincidences for orthogonal and parallel polarizations. Integrating the number of coincidences in a window around $\tau = 0$ for the two cases, we measure a raw HOM interference visibility $\mathcal{V}_{\text{raw}} = 1 - C_{\parallel}/C_{\perp} = 0.894(6)$. Accounting for the accidental coincidences with background events and the slight differences in the transmission and reflection coefficients of our combining beamsplitter gives a mode overlap of $0.982(7)$ (see [37]).

SOURCE EFFICIENCY

We measure a peak probability of $0.18(2)$ to generate a single photon into a single-mode fiber after polarization filtering and averaged for a 20% duty cycle. Accounting for optical losses and assuming that the single-photon has the same spatial mode as the 780-nm-write beam, we estimate a generation probability of $0.40(4)$ immediately after the atomic ensemble. The average probabilities go

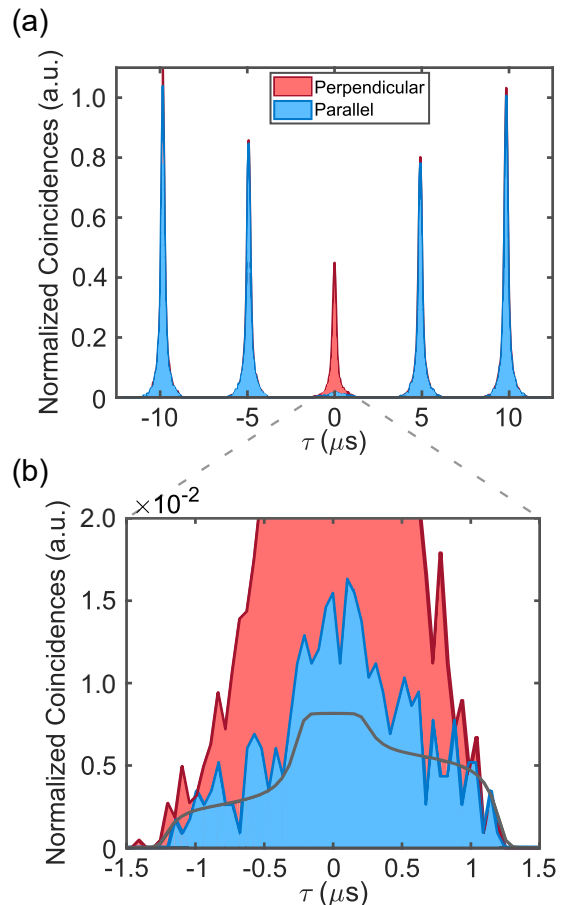


FIG. 3. Measured coincidences for indistinguishability characterization. (a) Normalized coincidences for HOM characterization with $4.92 \mu\text{s}$ cycle. Indistinguishable polarization states are represented in blue, and distinguishable polarization states are in red. (b) Normalized coincidences for HOM around $\tau = 0$, the grey line represents the background coincidences with 52-ns bins. All data shown were taken with 60% duty cycle.

down to $0.14(1)$ and $0.31(1)$, respectively for a 60% duty cycle.

We calculate $P_{\text{th}} = \eta_w \eta_s \eta_r$ as a product of the writing, η_w , storage, η_s , and retrieval, η_r , efficiencies to estimate the theoretical probability of generating a photon. Referring the reader to the Supplement [37] for the details of the theoretical analysis, we summarize it here only briefly. We simulate the writing of the spin wave using a Lindblad master equation to estimate the writing efficiency and the storage efficiency. We calculate the retrieval efficiency using the optical Maxwell-Bloch equations with the formalism in Ref. [38]. Using independently measured experimental values as input parameters, we obtain a theoretical prediction of $P_{\text{th}} \approx 0.42(3)$ (see Supplement [37]). This value is consistent with the measured generation probability for the longest pulsing periods, t_p .

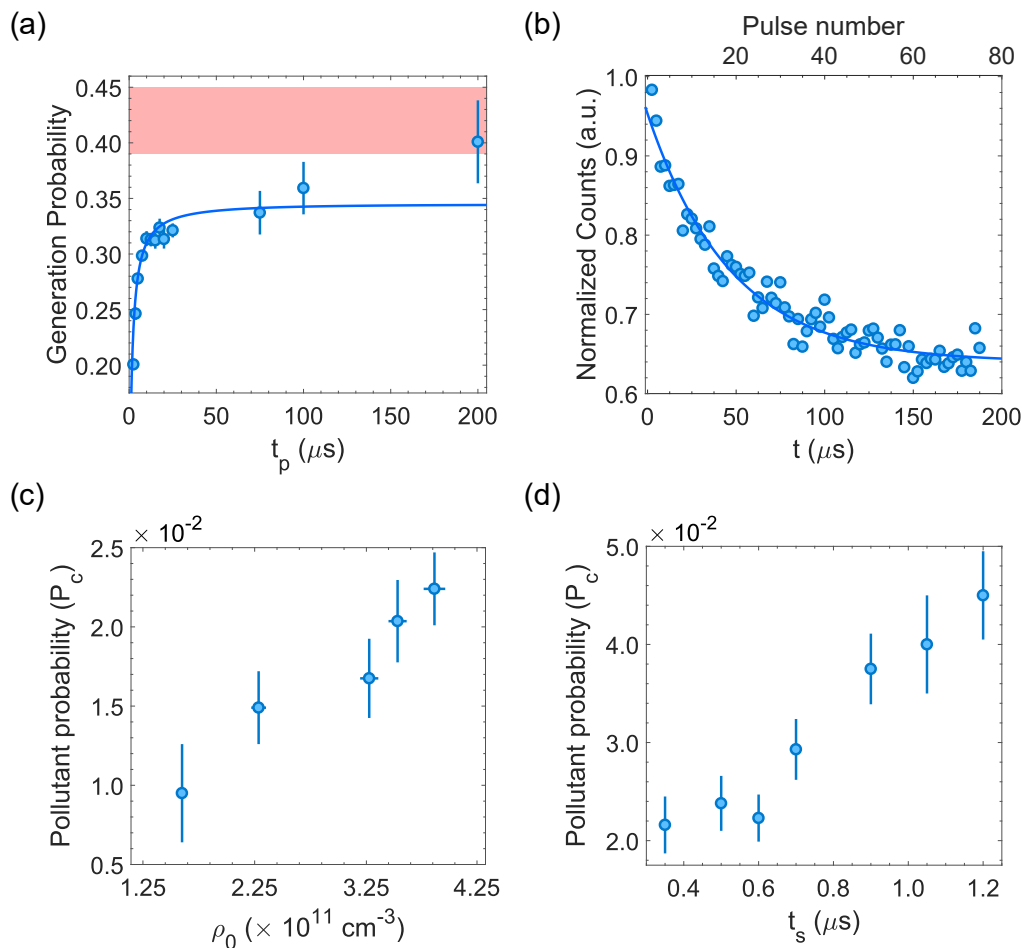


FIG. 4. Effect of contaminants on single-photon generation. (a) Photon generation probability as function of pulse period t_p . Dark-blue line is fitted using Eq. 1 in steady state for $n \rightarrow \infty$ using the values for P_c and τ_c in the main text, we obtain $P_{max} = 0.35(2)$. Red band shows the generation probability predicted by the theoretical model. (b) Normalized summed counts per pulse for a pulse train with $2.5\text{-}\mu\text{s}$ pulse period. Dark-blue line is fitted with Eq. 1. (c) P_c vs. peak atomic density ρ_0 with a fixed storage $t_s = 350 \text{ ns}$. (d) P_c vs. time t_s with a density $\approx 4 \times 10^{11} \text{ cm}^{-3}$.

We observed that the average photon production efficiency decreased at higher repetition rates, as shown in Figure 4(a). (Here the photon probability is determined immediately after the atom cloud by accounting for independently measured optical losses.) The initial pulse in a pulse series had higher efficiency, however, the efficiency of subsequent pulses decreased exponentially to the steady-state value on a $\approx 60 \mu\text{s}$ time scale [see Figure 4(b)].

These observations are consistent with the creation of contaminant atoms in other long-lived Rydberg states that are not removed by the retrieval field. These states interact strongly with the target Rydberg state, affecting subsequent writing events. Similar contaminant states have been observed in previous experiments [33, 39, 40], and have been analyzed extensively [41–44]. Once a contaminant is in the medium, it disables the writing of a spin wave for the later pulses. However, contaminants have a finite lifetime in the medium, therefore, the pho-

ton generation probability decreases for shorter pulse periods.

We use a simple model to capture the effect of contaminants on photon production (see [37] for details). We assume that for any given pulse, there is a probability P_c of creating a contaminant. If the contaminant state has a lifetime τ_c , then the probability P_n of having a contaminant in the n -th pulse of a pulse series with period t_p is

$$P_n = P_c \frac{1 - (e^{-t_p/\tau_c} - P_c)^n}{1 - e^{-t_p/\tau_c} + P_c}. \quad (1)$$

For $\tau_c \gg t_p$, the average contaminant probability as $n \rightarrow \infty$ can be significant, even if P_c is small. The probability $P_g(n)$ of successfully generating a single-photon on the n -th pulse in the presence of a contaminant is decreased according to $P_g(n) = P_{max}(1 - P_n)$, where P_{max} is the probability of photon generation in the absence of contaminants. The steady state efficiency is given by

$P_g(n \rightarrow \infty)$. Fitting this equation to pulse sequence data as shown in Fig. 4(b), we determine $P_c = 1.9(3) \times 10^{-2}$, and $\tau_c = 65(8) \mu\text{s}$, which is in good agreement with the data in Fig. 4(a).

We find that P_c increases linearly with atomic density ρ [see Fig. 4(c)], which suggests that the source of contaminants is ground-Rydberg interactions. For high principal quantum number, n , collisionally produced contaminants were identified in Ref [42] to be Rydberg states with principal quantum number $n - 4$ and quantum angular momentum $l > 2$. Furthermore, we find that P_c increases with storage time t_s at a rate $\approx 3 \times 10^{-2} \mu\text{s}^{-1}$, which gives a contaminant generation time-scale of $\approx 33 \mu\text{s}$ for a density $\approx 4 \times 10^{11} \text{ cm}^{-3}$. Contaminants are not a fundamental limitation since strong electric field pulses between writing pulses could be used to remove them.

We also note that for interrogation times longer than 100 ms, other effects such as heating and atom depolarization from rescattering become more significant, further reducing the photon generation for shorter t_p . However, these effects can be mitigated by detuning farther from the intermediate state.

SINGLE-MODE EFFICIENCY, RATE AND FIDELITY

There are many metrics used to quantify the various properties of single-photon sources. Optical quantum information schemes are susceptible to errors if they are not implemented with highly pure and indistinguishable single photons. In addition, scaling up quantum information protocols needs high generation efficiency, since any inefficiency will lead to an exponential decrease of the success probability with system size. Finally, the rate of single-photon production provides a limitation on the practicality of any protocol. To that end, we define three metrics that quantify these properties: \mathcal{F} , the single-photon fidelity, which is the fraction of emission that consists of a single photon in a single spectral, temporal, polarization, and spatial mode; η , the probability of generating a single photon in the desired mode; and \mathcal{R} , the brightness, which is the rate of photon production in the desired mode.

Assuming that the probability of multi-photon events greater than two is negligible, the only outcomes from a source are: single photons in the desired mode with probability η , single photons in an undesirable mode with probability P'_1 , two photons with probability P_2 , and null events with probability P_0 . Experimentally, we measure the following quantities: the overall emission efficiency, $P = 1 - P_0$; the HOM visibility, \mathcal{V} ; and the measure of the single-photon purity, $g^{(2)}$. These are given by:

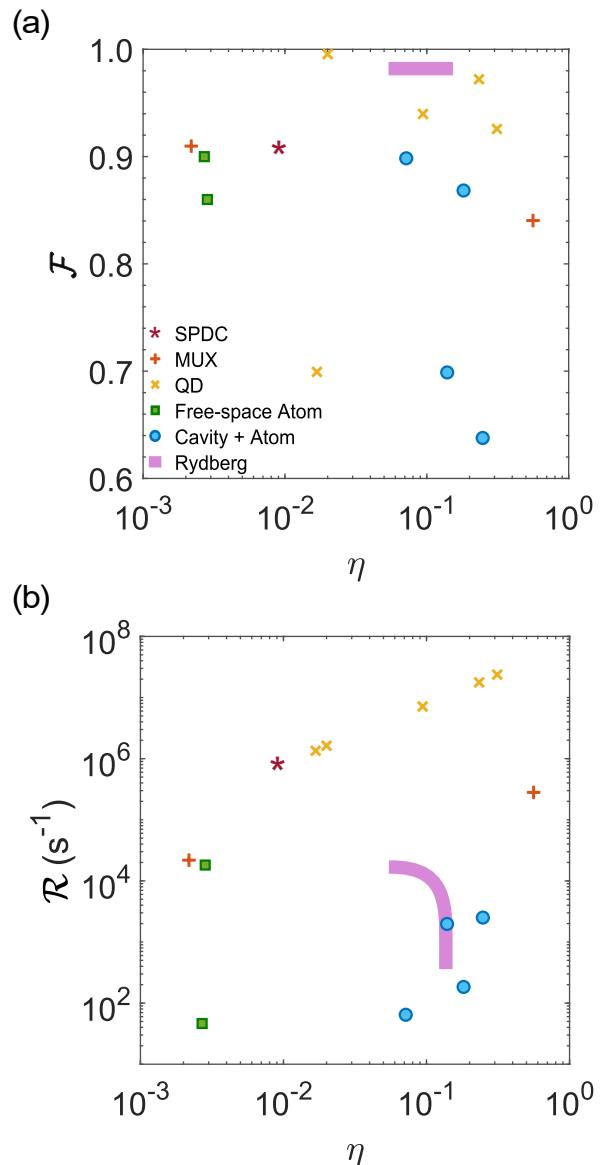


FIG. 5. Performance of a sample from different single-photon sources. Solid-state systems considered are spontaneous parametric down-conversion (SPDC) [45], multiplexed-heralded-single-photon source (MUX-HSPS) [46, 47] and quantum dots (QD) [48–52]. Atomic systems considered are single atoms in free-space [53, 54], atoms in cavities [55–58], and the Rydberg ensemble studied in this work (indicated in the purple line) accounting for the effect of different repetition rates for a duty cycle of 0.6. (For details on these sources, see tables in [37]). (a) Fidelity vs. single-mode efficiency. (b) Brightness vs. single-mode efficiency.

$$\begin{aligned}
 P &= 1 - P_0 = \eta + P'_1 + P_2, \\
 \mathcal{V} &= \frac{\eta}{\eta + P'_1}, \\
 g^{(2)} &\approx \frac{2P_2}{(\eta + P'_1 + 2P_2)^2},
 \end{aligned} \tag{2}$$

where we have assumed that the visibility \mathcal{V} is compensated for multi-photon events [37], and that these measurements are taken with standard non-number resolving photon counting detectors.

Solving the system of equations for η to second order in $g^{(2)}$, we get the single-mode efficiency η :

$$\eta = P\mathcal{V} \left(1 - \frac{1}{2}Pg^{(2)} \left(1 + Pg^{(2)} \right) \right). \quad (3)$$

We report the source brightness as $\mathcal{R} = R_{\text{eff}}\eta$, where R_{eff} is the clock rate weighted by the experimental duty cycle. Apart from source brightness, the rate at which undesirable emission is produced also matters for applications. We characterize this rate by the fidelity,

$$\mathcal{F} = 1 - \frac{P'_1 + P_2}{P} = \frac{\eta}{P}, \quad (4)$$

which is the fraction of collected emission that is made up of single photons in the correct mode. In Fig. 5 we show η , \mathcal{F} , and \mathcal{R} for a sample of different single-photon sources. Narrow bandwidth sources naturally compatible with coherent atomic systems are indicated with filled symbols.

CONCLUSION

By using the quantum nonlinearities of strongly interacting Rydberg states in a cold atomic ensemble, we demonstrated a single-photon source, operating with a 60% duty cycle, single-mode efficiency $\eta = 0.139(5)$, a single-mode brightness of $\mathcal{R} = 840(70) \text{ s}^{-1}$, and single-mode fidelity $\mathcal{F} = 0.982(7)$, this fidelity is the highest reported to our knowledge for an atomic-based source. Furthermore, we investigated the limitations of our current setup arising from nearby long-lived contaminant states.

Implementing feasible improvements to the current experiment we estimate that we can achieve up to $\eta \approx 0.4$ and moreover, ionizing pulses after each write-retrieval pulse to remove atoms in pollutant states may increase the brightness up to $\mathcal{R} \approx 1.2 \times 10^5 \text{ s}^{-1}$ without decreasing the duty cycle or the fidelity (see [37] for details). The efficiency could be further improved if the ensemble were coupled to a cavity [59]. Given their high efficiency, brightness, and fidelity, we have shown that single-photon sources based on Rydberg-atomic ensembles provide a promising platform for scalable quantum photonics. Furthermore, they are inherently compatible with narrow-bandwidth atomic platforms that have shown significant progress towards quantum information applications.

ACKNOWLEDGMENTS

All authors acknowledge support from the United States Army Research Lab's Center for Distributed Quantum Information (CDQI) at the University of Maryland and the Army Research Lab. A.C., D.O.-H., A.J.H., S.L.R., J.V.P., Y.W., P.B., and A.V.G. additionally acknowledge support from the National Science Foundation Physics Frontier Center at the Joint Quantum Institute (Grant No. PHY1430094). Y.W., P.B., and A.V.G. additionally acknowledge support from AFOSR, ARO MURI, and DoE ASCR Quantum Testbed Pathfinder program (award No. DE-SC0019040).

We are grateful to Mary Lyon for her significant contributions to the design and construction of the apparatus and Patrick Banner for his contributions to data collection. We also want to thank Luis A. Orozco for fruitful discussions.

-
- [1] J. Carolan, C. Harrold, C. Sparrow, E. Martín-López, N. J. Russell, J. W. Silverstone, P. J. Shadbolt, N. Matsuda, M. Oguma, M. Itoh, G. D. Marshall, M. G. Thompson, J. C. F. Matthews, T. Hashimoto, J. L. O'Brien, and A. Laing, "Universal linear optics," *Science* **349**, 711–716 (2015).
 - [2] H. Wang, J. Qin, X. Ding, M.-C. Chen, S. Chen, X. You, Y.-M. He, X. Jiang, L. You, Z. Wang, C. Schneider, J. J. Renema, S. Höfling, C.-Y. Lu, and J.-W. Pan, "Boson sampling with 20 input photons and a 60-mode interferometer in a 10^{14} -dimensional hilbert space," *Phys. Rev. Lett.* **123**, 250503 (2019).
 - [3] J. Yin, Y. Cao, Y.-H. Li, S.-K. Liao, L. Zhang, J.-G. Ren, W.-Q. Cai, W.-Y. Liu, B. Li, H. Dai *et al.*, "Satellite-based entanglement distribution over 1200 kilometers," *Science* **356**, 1140–1144 (2017).
 - [4] S. Slussarenko, M. M. Weston, H. M. Chrzanowski, L. K. Shalm, V. B. Verma, S. W. Nam, and G. J. Pryde, "Unconditional violation of the shot-noise limit in photonic quantum metrology," *Nature Photon* **11**, 700–703 (2017).
 - [5] Y. Wang, J. Li, S. Zhang, K. Su, Y. Zhou, K. Liao, S. Du, H. Yan, and S.-L. Zhu, "Efficient quantum memory for single-photon polarization qubits," *Nature Photon* **13**, 346–351 (2019).
 - [6] Y. Yu, F. Ma, X.-Y. Luo, B. Jing, P.-F. Sun, R.-Z. Fang, C.-W. Yang, H. Liu, M.-Y. Zheng, X.-P. Xie *et al.*, "Entanglement of two quantum memories via fibres over dozens of kilometres," *Nature* **578**, 240–245 (2020).
 - [7] M. Bock, P. Eich, S. Kucera, M. Kreis, A. Lenhard, C. Becher, and J. Eschner, "High-fidelity entanglement between a trapped ion and a telecom photon via quantum frequency conversion," *Nat Commun* **9**, 1–7 (2018).
 - [8] C. J. Ballance, T. P. Harty, N. M. Linke, M. A. Sepiol, and D. M. Lucas, "High-fidelity quantum logic gates using trapped-ion hyperfine qubits," *Phys. Rev. Lett.* **117**, 060504 (2016).
 - [9] C. Gross and I. Bloch, "Quantum simulations with ultracold atoms in optical lattices," *Science* **357**, 995–1001 (2017).

- [10] T. Peyronel, O. Firstenberg, Q.-Y. Liang, S. Hofferberth, A. V. Gorshkov, T. Pohl, M. D. Lukin, and V. Vuletić, “Quantum nonlinear optics with single photons enabled by strongly interacting atoms,” *Nature* **488**, 57–60 (2012).
- [11] D. Maxwell, D. Szwed, D. Paredes-Barato, H. Busche, J. D. Pritchard, A. Gauguier, K. J. Weatherill, M. Jones, and C. S. Adams, “Storage and control of optical photons using rydberg polaritons,” *Phys. Rev. Lett.* **110**, 103001 (2013).
- [12] L. Li and A. Kuzmich, “Quantum memory with strong and controllable rydberg-level interactions,” *Nat Commun* **7**, 13618 (2016).
- [13] A. Paris-Mandoki, C. Braun, J. Kumlin, C. Tresp, I. Mirgorodskiy, F. Christaller, H. P. Büchler, and S. Hofferberth, “Free-space quantum electrodynamics with a single rydberg superatom,” *Physical Review X* **7**, 041010 (2017).
- [14] Y. Dudin and A. Kuzmich, “Strongly interacting rydberg excitations of a cold atomic gas,” *Science* **336**, 887–889 (2012).
- [15] F. Ripka, H. Kübler, R. Löw, and T. Pfau, “A room-temperature single-photon source based on strongly interacting rydberg atoms,” *Science* **362**, 446–449 (2018).
- [16] H. Gorniaczyk, C. Tresp, J. Schmidt, H. Fedder, and S. Hofferberth, “Single-photon transistor mediated by interstate rydberg interactions,” *Phys. Rev. Lett.* **113**, 053601 (2014).
- [17] D. Tiarks, S. Baur, K. Schneider, S. Dürr, and G. Rempe, “Single-photon transistor using a förster resonance,” *Phys. Rev. Lett.* **113**, 053602 (2014).
- [18] H. Gorniaczyk, C. Tresp, P. Bienias, A. Paris-Mandoki, W. Li, I. Mirgorodskiy, H. Büchler, I. Lesanovsky, and S. Hofferberth, “Enhancement of rydberg-mediated single-photon nonlinearities by electrically tuned förster resonances,” *Nat Commun* **7**, 12480 (2016).
- [19] D. Tiarks, S. Schmidt, G. Rempe, and S. Dürr, “Optical π phase shift created with a single-photon pulse,” *Science Advances* **2**, e1600036 (2016).
- [20] J. D. Thompson, T. L. Nicholson, Q.-Y. Liang, S. H. Cantu, A. V. Venkatramani, S. Choi, I. A. Fedorov, D. Viscor, T. Pohl, M. D. Lukin *et al.*, “Symmetry-protected collisions between strongly interacting photons,” *Nature* **542**, 206–209 (2017).
- [21] D. Tiarks, S. Schmidt-Eberle, T. Stolz, G. Rempe, and S. Dürr, “A photon–photon quantum gate based on rydberg interactions,” *Nature Phys* **15**, 124–126 (2018).
- [22] K. Maller, M. Lichtman, T. Xia, Y. Sun, M. Piotrowicz, A. Carr, L. Isenhower, and M. Saffman, “Rydberg-blockade controlled-not gate and entanglement in a two-dimensional array of neutral-atom qubits,” *Physical Review A* **92**, 022336 (2015).
- [23] Y. Zeng, P. Xu, X. He, Y. Liu, M. Liu, J. Wang, D. Papoular, G. Shlyapnikov, and M. Zhan, “Entangling two individual atoms of different isotopes via rydberg blockade,” *Phys. Rev. Lett.* **119**, 160502 (2017).
- [24] H. Levine, A. Keesling, A. Omran, H. Bernien, S. Schwartz, A. S. Zibrov, M. Endres, M. Greiner, V. Vuletić, and M. D. Lukin, “High-fidelity control and entanglement of rydberg-atom qubits,” *Phys. Rev. Lett.* **121**, 123603 (2018).
- [25] A. N. Craddock, J. Hannegan, D. P. Ornelas-Huerta, J. D. Siverns, A. J. Hachtel, E. A. Goldschmidt, J. V. Porto, Q. Quraishi, and S. L. Rolston, “Quantum interference between photons from an atomic ensemble and a remote atomic ion,” *Phys. Rev. Lett.* **123**, 213601 (2019).
- [26] P. Schauß, M. Cheneau, M. Endres, T. Fukuhara, S. Hild, A. Omran, T. Pohl, C. Gross, S. Kuhr, and I. Bloch, “Observation of spatially ordered structures in a two-dimensional rydberg gas,” *Nature* **491**, 87–91 (2012).
- [27] J. Zeiher, J.-y. Choi, A. Rubio-Abadal, T. Pohl, R. van Bijnen, I. Bloch, and C. Gross, “Coherent many-body spin dynamics in a long-range interacting ising chain,” *Physical Review X* **7**, 041063 (2017).
- [28] V. Lienhard, S. De Léséleuc, D. Barredo, T. Lahaye, A. Browaeys, M. Schuler, L.-P. Henry, and A. M. Läuchli, “Observing the space-and time-dependent growth of correlations in dynamically tuned synthetic ising models with antiferromagnetic interactions,” *Physical Review X* **8**, 021070 (2018).
- [29] H. Kim, Y. Park, K. Kim, H.-S. Sim, and J. Ahn, “Detailed balance of thermalization dynamics in rydberg-atom quantum simulators,” *Phys. Rev. Lett.* **120**, 180502 (2018).
- [30] M. Saffman and T. G. Walker, “Creating single-atom and single-photon sources from entangled atomic ensembles,” *Phys. Rev. A* **66**, 065403 (2002).
- [31] M. D. Lukin, M. Fleischhauer, R. Cote, L. M. Duan, D. Jaksch, J. I. Cirac, and P. Zoller, “Dipole blockade and quantum information processing in mesoscopic atomic ensembles,” *Phys. Rev. Lett.* **87**, 037901 (2001).
- [32] N. Sangouard, C. Simon, H. de Riedmatten, and N. Gisin, “Quantum repeaters based on atomic ensembles and linear optics,” *Rev. Mod. Phys.* **83**, 33–80 (2011).
- [33] E. A. Goldschmidt, T. Boulier, R. C. Brown, S. B. Koller, J. T. Young, A. V. Gorshkov, S. L. Rolston, and J. V. Porto, “Anomalous broadening in driven dissipative rydberg systems,” *Phys. Rev. Lett.* **116**, 113001 (2016).
- [34] M. D. Eisaman, J. Fan, A. Migdall, and S. V. Polyakov, “Invited review article: Single-photon sources and detectors,” *Review of Scientific Instruments* **82**, 071101 (2011).
- [35] N. Šibalić, J. D. Pritchard, C. S. Adams, and K. J. Weatherill, “Arc: An open-source library for calculating properties of alkali rydberg atoms,” *Computer Physics Communications* **220**, 319–331 (2017).
- [36] Y. Dudin, L. Li, F. Bariani, and A. Kuzmich, “Observation of coherent many-body rabi oscillations,” *Nature Physics* **8**, 790–794 (2012).
- [37] Supplemental Material contains the details on experimental configuration, background subtraction, HOM visibility reduction discussion, contaminant states creation, theory model to estimate writing and retrieval efficiencies, possible improvements, and information about single-photon sources plotted in Fig. 5.
- [38] A. V. Gorshkov, A. André, M. D. Lukin, and A. S. Sørensen, “Photon storage in Λ -type optically dense atomic media. ii. free-space model,” *Phys. Rev. A* **76**, 033805 (2007).
- [39] B. J. DeSalvo, J. A. Aman, C. Gaul, T. Pohl, S. Yoshida, J. Burgdörfer, K. R. A. Hazzard, F. B. Dunning, and T. C. Killian, “Rydberg-blockade effects in autler-townes spectra of ultracold strontium,” *Phys. Rev. A* **93**, 022709 (2016).
- [40] D. P. Sadler, E. M. Bridge, D. Boddy, A. D. Bounds, N. C. Keegan, G. Lochead, M. P. A. Jones, and B. Olmos, “Radiation trapping in a dense cold rydberg gas,” *Phys. Rev. A* **95**, 013839 (2017).

- [41] J. A. Aman, B. J. DeSalvo, F. B. Dunning, T. C. Killian, S. Yoshida, and J. Burgdörfer, “Trap losses induced by near-resonant rydberg dressing of cold atomic gases,” *Phys. Rev. A* **93**, 043425 (2016).
- [42] M. Schlagmüller, T. C. Liebisch, F. Engel, K. S. Kleinbach, F. Böttcher, U. Hermann, K. M. Westphal, A. Gaj, R. Löw, S. Hofferberth, T. Pfau, J. Pérez-Ríos, and C. H. Greene, “Ultracold chemical reactions of a single rydberg atom in a dense gas,” *Phys. Rev. X* **6**, 031020 (2016).
- [43] T. Boulier, E. Magnan, C. Bracamontes, J. Maslek, E. A. Goldschmidt, J. T. Young, A. V. Gorshkov, S. L. Rolston, and J. V. Porto, “Spontaneous avalanche dephasing in large rydberg ensembles,” *Phys. Rev. A* **96**, 053409 (2017).
- [44] P. Bienias, J. Douglas, A. Paris-Mandoki, P. Titum, I. Mirgorodskiy, C. Tresp, E. Zeuthen, M. J. Gullans, M. Manzoni, S. Hofferberth, D. Chang, and A. V. Gorshkov, “Photon propagation through dissipative Rydberg media at large input rates,” arXiv e-prints arXiv:1807.07586 (2018).
- [45] X.-L. Wang, L.-K. Chen, W. Li, H.-L. Huang, C. Liu, C. Chen, Y.-H. Luo, Z.-E. Su, D. Wu, Z.-D. Li, H. Lu, Y. Hu, X. Jiang, C.-Z. Peng, L. Li, N.-L. Liu, Y.-A. Chen, C.-Y. Lu, and J.-W. Pan, “Experimental ten-photon entanglement,” *Phys. Rev. Lett.* **117**, 210502 (2016).
- [46] C. Xiong, X. Zhang, Z. Liu, M. J. Collins, A. Mahendra, L. Helt, M. J. Steel, D.-Y. Choi, C. Chae, P. Leong *et al.*, “Active temporal multiplexing of indistinguishable heralded single photons,” *Nat Commun* **7**, 10853 (2016).
- [47] F. Kaneda and P. G. Kwiat, “High-efficiency single-photon generation via large-scale active time multiplexing,” *Science Advances* **5**, eaaw8586 (2019).
- [48] N. Somaschi, V. Giesz, L. De Santis, J. Loredo, M. P. Almeida, G. Hornecker, S. L. Portalupi, T. Grange, C. Antón, J. Demory *et al.*, “Near-optimal single-photon sources in the solid state,” *Nature Photon* **10**, 340–345 (2016).
- [49] J. C. Loredo, N. A. Zakaria, N. Somaschi, C. Anton, L. de Santis, V. Giesz, T. Grange, M. A. Broome, O. Gazzano, G. Coppola, I. Sagnes, A. Lemaitre, A. Auffeves, P. Senellart, M. P. Almeida, and A. G. White, “Scalable performance in solid-state single-photon sources,” *Optica* **3**, 433–440 (2016).
- [50] H. Wang, Y. He, Y.-H. Li, Z.-E. Su, B. Li, H.-L. Huang, X. Ding, M.-C. Chen, C. Liu, J. Qin *et al.*, “High-efficiency multiphoton boson sampling,” *Nature Photon* **11**, 361–365 (2017).
- [51] G. Kiršanskė, H. Thyrrstrup, R. S. Daveau, C. L. Dreeßen, T. Pregolato, L. Midolo, P. Tighineanu, A. Javadi, S. Stobbe, R. Schott, A. Ludwig, A. D. Wieck, S. I. Park, J. D. Song, A. V. Kuhlmann, I. Söllner, M. C. Löbl, R. J. Warburton, and P. Lodahl, “Indistinguishable and efficient single photons from a quantum dot in a planar nanobeam waveguide,” *Phys. Rev. B* **96**, 165306 (2017).
- [52] H. Wang, Y.-M. He, T.-H. Chung, H. Hu, Y. Yu, S. Chen, X. Ding, M.-C. Chen, J. Qin, X. Yang *et al.*, “Towards optimal single-photon sources from polarized microcavities,” *Nature Photon* **13**, 770–775 (2019).
- [53] P. Maunz, D. Moehring, S. Olmschenk, K. Younge, D. Matsukevich, and C. Monroe, “Quantum interference of photon pairs from two remote trapped atomic ions,” *Nature Phys* **3**, 538–541 (2007).
- [54] W. Rosenfeld, D. Burchardt, R. Garthoff, K. Redeker, N. Ortel, M. Rau, and H. Weinfurter, “Event-ready bell test using entangled atoms simultaneously closing detection and locality loopholes,” *Phys. Rev. Lett.* **119**, 010402 (2017).
- [55] J. K. Thompson, J. Simon, H. Loh, and V. Vuletić, “A high-brightness source of narrowband, identical-photon pairs,” *Science* **313**, 74–77 (2006).
- [56] T. Wilk, S. C. Webster, H. P. Specht, G. Rempe, and A. Kuhn, “Polarization-controlled single photons,” *Phys. Rev. Lett.* **98**, 063601 (2007).
- [57] P. B. R. Nisbet-Jones, J. Dille, D. Ljunggren, and A. Kuhn, “Highly efficient source for indistinguishable single photons of controlled shape,” *New Journal of Physics* **13**, 103036 (2011).
- [58] M. Mücke, J. Bochmann, C. Hahn, A. Neuzner, C. Nölleke, A. Reiserer, G. Rempe, and S. Ritter, “Generation of single photons from an atom-cavity system,” *Phys. Rev. A* **87**, 063805 (2013).
- [59] L. W. Clark, N. Jia, N. Schine, C. Baum, A. Georgakopoulos, and J. Simon, “Interacting floquet polaritons,” *Nature* **571**, 532–536 (2019).

SUPPLEMENTAL MATERIAL

Detailed experimental configuration

All the experiments are carried out with $\approx 10^4$ ^{87}Rb atoms trapped in a three-beam-crossed optical dipole trap with 1003-nm wavelength. Two of the beams form a $\approx \pm 11^\circ$ with respect to the x -axis (along the probe direction), while a third elliptical shaped beam travels in the y -axis, with all beams in the same (x - y) plane. The relative powers of the dipole beams are adjusted so that the RMS dimensions of the trapped atomic cloud are $\sigma_r = 20$ μm in the radial direction and $\sigma_x = 27$ μm .

The initial trapping and cooling take place in a magneto-optical trap (MOT). For most experiments, we load for 250 ms; if we need to adjust the atomic medium optical density (OD), we change the loading time, ranging from 50 ms to 1500 ms (with OD up to ≈ 16). Afterward, we perform a compressed-MOT stage by ramping-up the magnetic field gradient, while at the same time slowly ramping-up the dipole trap power.

We further cool the atoms to ≈ 10 μK using a gray molasses [S1].

Next, we optically pump the atoms into the $|5S_{1/2}, F = 2, m_F = 2\rangle$ state, using σ_+ polarized light blue-detuned from the $F = 2$ to $F' = 2$, D1 transition. We then couple the ground and Rydberg state with a two-photon transition. A 780-nm weak-probe field addresses the transition from the ground state, $|5S_{1/2}, F = 2, m_F = 2\rangle$ to the intermediate state, $|5P_{3/2}, F = 3, m_F = 3\rangle$; a strong-control field addresses the transition from the intermediate state to the Rydberg state, $|139S_{1/2}, J = 1/2, m_J = 1/2\rangle$ with a wavelength of 479 nm.

Both the probe and control lasers are frequency stabilized via an ultra-low expansion (ULE) cavity with a linewidth < 10 kHz. We use probe light that has been transmitted and filtered by the ULE cavity to reduce phase noise [S2], .

There are eight electrodes in vacuum that allow for control of local electric fields. With this configuration, we cancel DC-Stark shifts to tens of kHz level in all three directions, shifts that would otherwise tune the Rydberg state out of resonance due to the large polarizability of the 139S state, $\alpha_{139S} \approx 61$ GHz/(V/cm) 2 [S3].

The axial RMS of the atomic cloud, $\sigma_x \approx 27$ μm is smaller than the blockade radius, $r_b \approx 60$ μm to suppress the creation of multiple Rydberg atoms. Additionally, we focus the probe beam down to a $1/e^2$ waist of $w_p \approx 3.3$ μm to ensure the system is effectively uni-dimensional ($w_p \leq r_b$). The control beam is counter-propagating to the probe and focused to a beam waist of $w_c \approx 19$ μm . The larger beam waist provides an approximately uniform control field across the probe area. After exiting the chamber, the probe light passes through a polarization beam splitter (PBS), and a set of bandpass filters centered at 780-nm, a narrow 1-nm bandwidth filter (Alluxa 780-1 OD6[?]), and a broader 12.5-nm bandwidth filter (Semrock LL01-780-12.5), before being coupled into a single-mode polarization-maintaining fiber (PMF). Then, the light is sent to a Hong-Ou-Mandel (HOM) interferometer, which has another set of broad filters in front of the single-mode fibers (SMF) that send the light to the single-photon avalanche detectors (SPAD) (Excelitas SPCM-780-13).

We write a spin wave by pulsing the probe and the control field for ≈ 370 ns. The peak Rabi frequencies are $\Omega_p \approx 2\pi \times 1$ MHz and $\Omega_c \approx 2\pi \times 7$ MHz, respectively. Both fields are detuned from the intermediate state by $\Delta_p \approx 2\pi \times 50$ MHz, with the two-photon transition close to resonance. Due to the collective nature from the blocked excitation [S4], there is a $\sqrt{N} \approx 20$ enhancement to the two-photon Rabi frequency, $\sqrt{N}\Omega_{2\text{-photon}} = \sqrt{N}\Omega_p\Omega_c/(2\Delta_p)$, inferred from the π -time. This enhancement corresponds to an $\text{OD} \approx 13$ given the blocked volume.

After writing, we turn off the addressing lasers and hold (store) the spin wave in the medium for ≈ 350 ns; this is the minimum time required to switch the control acousto-optic modulator (AOM) frequency. We turn on the control field blue-detuned from the intermediate state by $\Delta_c \approx 2\pi \times 7$ MHz to map the spin wave into a single photon. We use an AOM before the PMF as a hardware gate to avoid saturating the SPADs from the initial write pulse.

We measure the optical losses along the path of the probe light to characterize the generation efficiency in Table S1.

Element	Efficiency
Optics transmission	0.75(2)
AOM diffraction	0.79(2)
PMF coupling	0.75(2)
HOM-interferometer	0.38(1)
SPAD	0.67(1)

TABLE S1. List of the efficiencies along the probe path.

The propagation efficiency includes all the optical elements, such as filters, dichroics, mirrors, polarizing beam splitters, mirrors, and lenses. With realistic improvements on higher transmission coatings and using an electro-optical modulator instead of an AOM, we could get an efficiency up to 0.65 after the PMF, from the current 0.44.

Background subtraction

For all our single-photon measurements, we use two SPADs, with average background rates of $\approx 80 \text{ s}^{-1}$, and, $\approx 100 \text{ s}^{-1}$. This count rate is due to detector dark counts and leakage of ambient light.

Since the photons arrive at the detectors at a known time, we apply a gate corresponding to a $1.4 \mu\text{s}$ time window, which contains more than 99.9% of the pulse. We implement this in software to extract the background-photon and background-background coincidence rates from counts outside this window. With this information, we can determine the temporal profile of the accidental coincidences, which we subtract from the data. The probability of a background coincidence, c_{back} , is the sum of the products of single event rates:

$$c_{\text{back}}(t_1, t_2) = P_1(t_1)B_2(t_2) + B_1(t_1)P_2(t_2) + B_1(t_1)B_2(t_2), \quad (\text{S1})$$

where t_1 and t_2 are absolute times relative to some clock, for SPAD 1 and 2 respectively. $P_i(t_i)$, is the probability per unit time of a photon detection event at detector i , and $B_i(t_i)$ is the probability per unit time of a background. Changing to the relative time coordinate, $\tau = t_2 - t_1$, the background coincidence probability is,

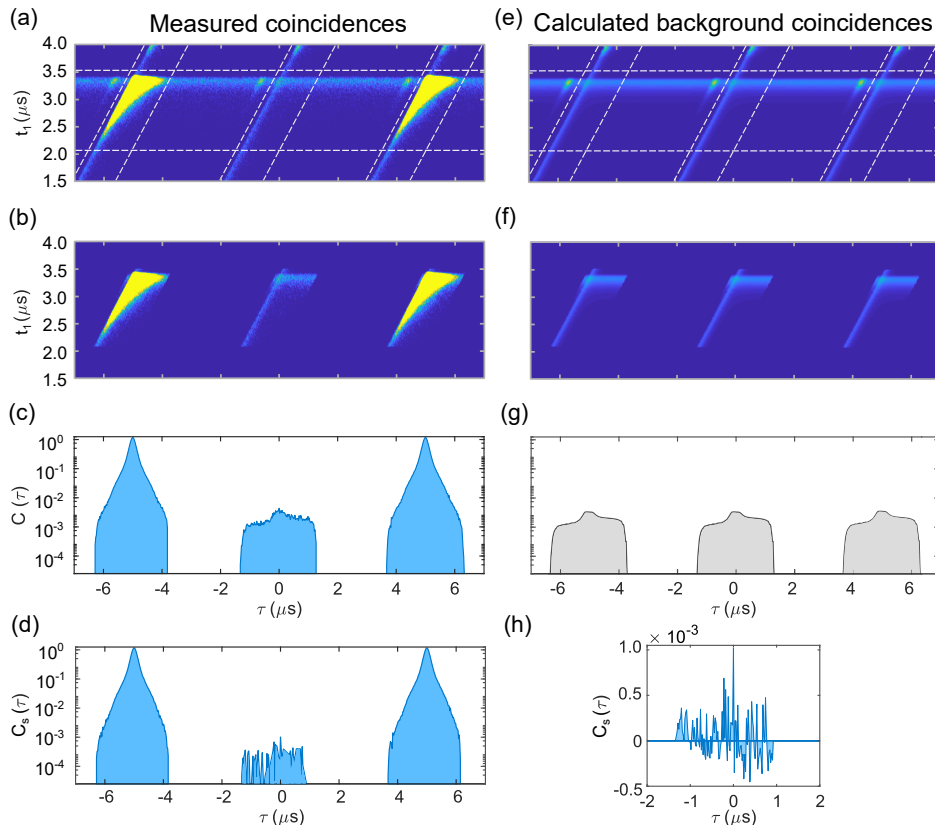


FIG. S1. Reconstruction of coincidences given the background and photon rate measured at each detector. (a) Raw data coincidences as a function of absolute time t_1 , for SPAD 1 and τ , the relative time between both SPADs. White-dashed lines indicate the position of the gating window for each repetition cycle. (b) Data with gate applied. (c) Total coincidence rate after applying the gate as a function of τ . (d) Photon-photon coincidence rate after subtracting the background from the data. (e) Calculated background coincidences as a function of t_1 and τ , based on the measured single-event rates $P_i(t)$ and B_i . (f) Calculated background coincidences after the gate. (g) Background coincidence rate as a function of τ . (h) Zoom around $\tau = 0$ of background-subtracted data in linear scale.

$$c_{\text{back}}(t_1, \tau) = P_1(t_1)B_2(\tau + t_1) + B_1(t_1)P_2(\tau + t_1) + B_1(t_1)B_2(\tau + t_1). \quad (\text{S2})$$

We integrate t_1 over a time window $t_{\text{end}} - t_{\text{start}}$ to obtain the total background coincidence rate as a function of the relative time, τ :

$$C_{\text{back}}(\tau) = \int_{t_{\text{start}}}^{t_{\text{end}}} dt_1 [P_1(t_1)B_2(\tau + t_1) + B_1(t_1)P_2(\tau + t_1) + B_1(t_1)B_2(\tau + t_1)], \quad (\text{S3})$$

where, t_{start} , is synchronized to the photon arrival. With the gate, the background and pulse probability have a time dependence

$$B_1(t_1), P_1(t_1) = \begin{cases} B_1, P_1(t_1) & \text{for } t_{\text{start}} \leq t_1 \leq t_{\text{end}} \\ 0 & \text{otherwise} \end{cases}$$

$$B_2(\tau + t_1), P_2(\tau + t_1) = \begin{cases} B_2, P_2(\tau + t_1) & \text{for } t_1 - t_{\text{end}} \leq \tau \leq t_1 - t_{\text{start}} \\ 0 & \text{otherwise} \end{cases}$$

With the independently measured single event rates $P_i(t)$ and B_i , we calculate $C_{\text{back}}(\tau)$.

This process is shown graphically in Figure S1, where C_{back} are the total coincidences rate from photon-background and background-background around $\tau = 0$. Finally Figure S1(h) shows the background subtracted coincidences rate, $C_s(\tau)$, within the gate window.

HOM visibility discussion

If two single photons are incident simultaneously on separate ports a_1 and a_2 of a perfect 50:50 beamsplitter (BS) the initial state $|1_1, 1_2\rangle$, becomes:

$$|1_1, 1_2\rangle \rightarrow \frac{1}{\sqrt{2}}(|2_3, 0_4\rangle + |0_3, 2_4\rangle) \quad (\text{S4})$$

where a_3, a_4 are the output ports and we assumed that the input photons are in pure states and indistinguishable from each other. In this case, the probability of a coincidence detection is zero and the HOM visibility is one. In practice, the following factors reduce the visibility from its maximum value [S5]:

- one or both photons are not in a pure state,
- there is more than one photon at either BS input port,
- an imperfect 50:50 BS.

We will focus on the effect of the last two conditions: multi-photon events and imperfect BS.

Following the discussion from [S6], we define the scattering matrix, S for a general BS as,

$$S = \begin{pmatrix} t_1 & r_2 e^{i\phi_2} \\ r_1 e^{i\phi_1} & t_2 \end{pmatrix}, \quad (\text{S5})$$

where r_1 (r_2), t_1 (t_2), are the reflection and transmission amplitudes with a relative phase ϕ_1 (ϕ_2) for port 1 (2).

Then the input-output relations of the BS, ignoring any frequency dependence:

$$\begin{pmatrix} \hat{a}_3 \\ \hat{a}_4 \end{pmatrix} = \begin{pmatrix} t_1 & r_2 e^{i\phi_2} \\ r_1 e^{i\phi_1} & t_2 \end{pmatrix} \begin{pmatrix} \hat{a}_1 \\ \hat{a}_2 \end{pmatrix}, \quad (\text{S6})$$

where \hat{a}_i are the photon ladder operator for the input and output ports. Generally, the scattering matrix, S , is not unitary.

For a lossy BS, where the output fields total energy is lower than the input fields energy, the following inequality holds:

$$\sqrt{t_1^2 r_2^2 + r_1^2 t_2^2 + 2t_1 r_1 t_2 r_2 \cos \alpha} \leq \sqrt{(1 - t_1^2 - r_1^2)(1 - t_2^2 - r_2^2)}, \quad (\text{S7})$$

where $\alpha = \phi_1 + \phi_2$, affects the maximum value that the visibility can attain. The phase, α , is constrained by energy conservation, and we assume $\alpha = \pi$.

The number operator for the input ports 1 and 2 (output 3 and 4) is $\hat{n}_i = \hat{a}_i^\dagger \hat{a}_i$. Assuming that the probability of states with more than two photons is negligible, the coincidence probability, $P(1_3, 1_4)$,

$$\begin{aligned} P(1_3, 1_4) &= \langle \hat{n}_3 \hat{n}_4 \rangle \\ &= \langle t_1^2 r_1^2 \hat{n}_1^2 + t_2^2 r_2^2 \hat{n}_2^2 + (t_1^2 t_2^2 + r_1^2 r_2^2 - 2t_1 r_1 t_2 r_2) \hat{n}_1 \hat{n}_2 \rangle \\ &= (t_1^2 r_1^2 + t_2^2 r_2^2) 2P_2 + (t_1^2 t_2^2 + r_1^2 r_2^2 - 2ct_1 r_1 t_2 r_2) P_1^2. \end{aligned} \quad (\text{S8})$$

Here P_1 is the probability of a single photon, P_2 is the probability of two photons at one input port, and c is the mode overlap of the two incident photons. Following the assumption that the probability of more than two-photon states is negligible, we can rewrite P_2 as a function of the correlation function $g^{(2)}(0)$ and P_1 , as $P_2 \approx g^{(2)}(0)P_1^2/2$. The coincidence probability:

$$P(1_3, 1_4) \approx \left[t_1^2 t_2^2 + r_1^2 r_2^2 + (t_1^2 r_1^2 + t_2^2 r_2^2) g^{(2)} - 2ct_1 r_1 t_2 r_2 \right] P_1^2. \quad (\text{S9})$$

For the more general case, where the BS coefficients are not the same for orthogonal polarizations, H , and V

$$\begin{aligned} \mathcal{V} &= \frac{P(1_3, 1_4)_{HV}|_{c=0} - P(1_3, 1_4)_{HH}|_{c=c}}{P(1_3, 1_4)_{HV}|_{c=0}} \\ &= \frac{t_{1V}^2 t_{2H}^2 + r_{1V}^2 r_{2H}^2 - t_{1H}^2 t_{2H}^2 - r_{1H}^2 r_{2H}^2 + (t_{1V}^2 r_{1V}^2 - t_{1H}^2 r_{1H}^2) g^{(2)} + 2ct_{1H} r_{1H} t_{2H} r_{2H}}{t_{1V}^2 t_{2H}^2 + r_{1V}^2 r_{2H}^2 + (t_{1V}^2 r_{1V}^2 + t_{2H}^2 r_{2H}^2) g^{(2)}}, \end{aligned} \quad (\text{S10})$$

where we assume that in the case of $P(1_3, 1_4)_{HV}$, the photon at port 1 has H -polarization and the photon at port 2 has V -polarization, similarly for $P(1_3, 1_4)_{HH}$, both incoming photons have H -polarization.

In the particular case of a BS with symmetric ports, $t_1^2 = t_2^2 = T$ and, $r_1^2 = r_2^2 = R$, the visibility reduces to:

$$\mathcal{V} = \frac{2c}{T/R + R/T + 2g^{(2)}}. \quad (\text{S11})$$

If $T = R = 1/2$ and $g^{(2)}(0) = 0$, then the visibility is equal to the incoming photons overlap, c .

In the following table, we show the measured transmission and reflection coefficients of the BS used in the HOM characterization, for both H - and V -polarization:

Port/Polarization	T	R
Port 1 H	0.502(5)	0.421(3)
Port 1 V	0.484(5)	0.428(3)
Port 2 H	0.511(9)	0.426(5)

TABLE S2. Transmission and reflection coefficients for the BS used in the HOM interferometer.

We measured a background-subtracted visibility to be $\mathcal{V} = 0.966(6)$, and using equation (13) to take into account the imperfect BS, we find a mode overlap of 0.982(7).

Contaminants

We use a simple model to characterize the effects of the contaminants on the photon generation, where there is a probability that a stored spin wave is converted to a contaminant. Once a contaminant is present in the medium, it

disables the writing and storing of a spin wave until the contaminant decays, with a time constant τ_c . If P_c is the probability of creating a contaminant on a given pulse, then the probability, P_n , of a contaminant being present at pulse n depends on whether one was created in one of the previous pulses and remained to the n -th pulse

$$P_n = P_{n-1}e^{-t_p/\tau_c} + (1 - P_{n-1})P_c, \quad (\text{S12})$$

where t_p is the pulse spacing. If we set the initial condition to be $P_1 = P_c$, and use the identity, $(1-x) \sum_{j=0}^{n-1} x^j = 1-x^n$, we get the expression:

$$P_n = P_c \frac{1 - (e^{-t_p/\tau_c} - P_c)^n}{1 - e^{-t_p/\tau_c} + P_c}. \quad (\text{S13})$$

Then, the probability of successfully generating a photon, $P_g(n)$ is

$$P_g(n) = P_{max}(1 - P_n) = P_{max} \left(1 - P_c \frac{1 - (e^{-t_p/\tau_c} - P_c)^n}{1 - e^{-t_p/\tau_c} + P_c} \right), \quad (\text{S14})$$

where P_{max} is the maximum probability of generating a photon. For $n \rightarrow \infty$, the steady state probability P_s ,

$$P_s \approx P_{max} \left(1 - \frac{P_c}{1 - e^{-t_p/\tau_c} + P_c} \right). \quad (\text{S15})$$

We also model how the correlation function, $g^{(2)}(m t_p)$ for integer $m \neq 0$, is modified due to contaminants:

$$\begin{aligned} g^{(2)}(|m|t_p) &= \frac{\langle P_s P_g(m) \rangle}{\langle P_s^2 \rangle} \\ &= 1 + P_c \frac{(e^{-t_p/\tau_c} - P_c)^n}{1 - e^{-t_p/\tau_c}}, \end{aligned} \quad (\text{S16})$$

this manifests as a bunching feature around $\tau = 0$.

Theoretical model

Write and storage efficiency

We model the spin-wave as a super-atom with N -atoms being collectively driven into a single excitation to the Rydberg state, for the writing and storage time. The energy levels and decay rates of the super-atom are shown in Figure S2.

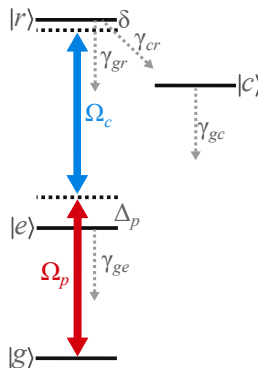


FIG. S2. Atomic levels showing the driving fields and decay rates used in theoretical model. Here we show the ground-state, as $|g\rangle = |5S_{1/2}\rangle$, the intermediate state $|e\rangle = |5P_{3/2}\rangle$, Rydberg state $|r\rangle = |139S_{1/2}\rangle$, and the contaminants states as $|c\rangle$.

We simulated the writing stage as driving the super-atom from the ground to the Rydberg state, with \sqrt{N} -enhanced Rabi frequency. During the writing time, t_w , the Rabi frequencies, $\Omega_p \approx 2\pi \times 1.0(2)$ MHz and $\Omega_c \approx 2\pi \times 6.8(3)$ MHz are kept constant. For the storage time, t_s , these driving frequencies are set to zero.

The Hamiltonian describing the the system depicted in Fig S2 in the rotating wave approximation is given by:

$$H(t) = \frac{\hbar}{2} \begin{pmatrix} 0 & \sqrt{N}\Omega_p(t) & 0 & 0 \\ \sqrt{N}\Omega_p(t) & -2\Delta_p & \Omega_c(t) & 0 \\ 0 & \Omega_c(t) & -2\delta & 0 \\ 0 & 0 & 0 & 0 \end{pmatrix}, \quad (\text{S17})$$

in the basis of $|g\rangle$, $|e\rangle$, $|r\rangle$, $|c\rangle$, for the ground, intermediate, Rydberg and contaminant state, respectively.

Using the Python package QuTip [S7], we calculated the non-unitary dynamics of this first stage using the master equation for the four level density matrix ρ :

$$\dot{\rho} = -\frac{i}{\hbar}[H, \rho] - \sum_n \frac{1}{2}\{\rho, C_n^\dagger C_n\} + C_n \rho C_n^\dagger, \quad (\text{S18})$$

where $C_1 = \sqrt{\gamma_{ge}}|g\rangle\langle e|$, $C_2 = \sqrt{\gamma_{gr}}|g\rangle\langle r|$, $C_3 = \sqrt{\gamma_{cr}}|c\rangle\langle r|$, and $C_4 = \sqrt{\gamma_{gc}}|g\rangle\langle c|$ are the jump operators.

Given the decay rates of the different states: $\gamma_{ge} \approx 2\pi \times 6.9(6)$ MHz, $\gamma_{gr} \approx 2\pi \times 88(6)$ kHz, $\gamma_{cr} \approx 2\pi \times 5(1)$ kHz, and $\gamma_{gc} \approx 2\pi \times 2.5(3)$ kHz, we calculate that the writing and storage efficiency are $\eta_w = 0.82(1)$, $\eta_s = 0.82(1)$, respectively.

Retrieval efficiency

We follow the derivations in Ref. [S8] to compute the retrieval efficiency. In the rescaled unit-less coordinates, $\tilde{z} = 0$ and $\tilde{z} = 1$ represent the front and the end of the atomic cloud, respectively. Suppose all atoms are in the $|r\rangle$ state in the beginning of the retrieval stage at time $\tilde{t} = 0$, the shape of the spin wave is given by $S(\tilde{z}, \tilde{t} = 0) = 1$ for $\tilde{z} \in [0, 1]$ and $S(\tilde{z}, \tilde{t} = 0) = 0$ for \tilde{z} elsewhere. The retrieval efficiency can be expressed in terms of the photon field $\mathcal{E}(\tilde{z}, \tilde{t})$ emitted by the stored spin wave at the end of the atomic cloud:

$$\eta_r = \int_0^\infty d\tilde{t} |\mathcal{E}(\tilde{z} = 1, \tilde{t})|^2. \quad (\text{S19})$$

$\mathcal{E}(1, \tilde{t})$ can be calculated as:

$$\mathcal{E}(1, \tilde{t}) = -\sqrt{d}\tilde{\Omega}(\tilde{t}) \exp(-\tilde{\gamma}_s \tilde{t}) \int_0^1 d\tilde{z} \frac{1}{1+i\tilde{\Delta}} e^{-(h(0, \tilde{t})+d\tilde{z})/(1+i\tilde{\Delta})} I_0 \left(2 \frac{\sqrt{h(0, \tilde{t})d\tilde{z}}}{1+i\tilde{\Delta}} \right) S(1-\tilde{z}), \quad (\text{S20})$$

where we define dimensionless parameters $d = \text{OD}/2$, $\tilde{\gamma}_s = (\gamma_{gr} + \gamma_{cr})/\gamma_{ge}$, $\tilde{\Delta} = 2\Delta_p/\gamma_{ge}$, $\tilde{\Omega}(t) = \Omega_c(t)/\gamma_{ge}$. $h(\tilde{t}, \tilde{t}') = \int_{\tilde{t}}^{\tilde{t}'} |\tilde{\Omega}(\tilde{t}'')|^2 d\tilde{t}''$ and I_0 is the 0th-order modified Bessel function of the first kind. When the control field Ω_c is constant in time, we define the dimensionless parameter $x_s = 2\tilde{\gamma}_s/|\tilde{\Omega}_c|^2$ which characterizes the strength of the decay rate compared to the control field. (S19) can be evaluated as

$$\eta_r = \int_0^1 d\tilde{z} \int_0^1 d\tilde{z}' K_r S(1-\tilde{z}) S^*(1-\tilde{z}'), \quad (\text{S21})$$

where K_r is given by

$$K_r = \frac{df(x_s)}{2} \exp \left[-\frac{df(x_s)}{2} \left((1+x_s(1-i\tilde{\Delta}))\tilde{z} + (1+x_s(1+i\tilde{\Delta}))d\tilde{z}' \right) \right] I_0(d\sqrt{\tilde{z}\tilde{z}'} f(x_s)), \quad (\text{S22})$$

and $f(x_s) = \frac{2}{2+x_s(1+\tilde{\Delta}^2)}$.

Evaluating the integral in Eq. (S21) numerically, we obtain the retrieval efficiency $\eta_r = 0.63(2)$. With these results, we estimate that the photon generation probability at the end of the cloud is $P_{\text{th}} = 0.42(3)$.

Possible improvements

With conservative feasible experimental improvements, such as implementing a ground-state blue-detuned optical dipole trap, as well as increasing the following parameters: $\Omega_c = 2\pi \times 10$ MHz, $\Delta_p = 2\pi \times 100$ MHz and OD=20, while decreasing the spin wave dephasing by a factor of two, we estimate that we could increase our probabilities up to $\eta_w\eta_s = 0.86$ and $\eta_r = 0.72$, while maintaining a relatively low contaminant probability, $P_c \approx 3 \times 10^{-2}$.

From the theoretical model, the main limiting factor is the retrieval process; in principle, the retrieval efficiency increases with higher OD; however, the contaminant production also grows with OD. A Rydberg ensemble with low OD coupled to a cavity could further increase light-matter interactions and therefore increase the overall photon production probability, making it a promising platform for scalable quantum information applications.

Single-photon sources

In Tables S3 and S4, there is detailed information about the properties of a representative sample of single-photon sources plotted in Fig. 5. in the main text. The notation, R , repetition rate, P is the probability of coupling a single-photon into a single-mode fiber, V , is the indistinguishability, η is the single-mode probability, \mathcal{R} is the brightness, and \mathcal{F} is the fidelity.

Type	Ref	R (MHz)	P	V	$g^{(2)}$	η	\mathcal{R} $\times 10^6 (s^{-1})$	\mathcal{F}
SPDC	[S9]	76	≈ 0.01	0.91	0.09	0.009	0.69	0.910
MUX	[S10]	10	≈ 0.002	0.91	~ 0.2	0.002	0.02	0.910
MUX	[S11]	0.5	0.667	0.91	0.269	0.561	0.28	0.840
QD	[S12]	82	≈ 0.02	0.996	0.024	0.020	1.63	0.996
QD	[S13]	80	0.024	0.7	0.013	0.017	1.34	0.699
QD	[S14]	76	0.337	0.93	0.027	0.312	23.71	0.926
QD	[S15]	76	0.10	0.94	0.006	0.094	7.14	0.940
QD	[S16]	76	0.24	0.975	0.025	0.233	17.7	0.972

TABLE S3. Table comparing the performances of solid state single-photon sources: spontaneous parametric down conversion (SPDC), multiplexed-heralded-single-photon source (MUX) and, quantum dot (QD). Values estimated from available data.

Type	Ref	Duty Cycle (%)	R (MHz)	P	V	$g^{(2)}$	η	\mathcal{R} $\times 10^3 (s^{-1})$	\mathcal{F}
Yb ion	[S17]	80	8	0.003	0.86	$\sim 10^{-3}$	0.003	18.16	0.860
Rb Atom	[S18]	33	0.052	0.003	0.9	$\sim 10^{-3}$	0.003	0.05	0.899
Ensemble in cavity	[S19]	≈ 1.8	0.05	0.08	0.9	0.05	0.072	0.06	0.898
Atom in cavity	[S20]	≈ 2	0.7	0.2	0.7	$\sim 10^{-2}$	0.140	1.96	0.699
Atom in cavity	[S21]	0.1	1	0.21	0.87	0.02	0.182	0.18	0.868
Atom in cavity	[S22]	100	0.01	0.39	0.64	0.02	0.249	2.49	0.637
Rydberg	this work	60	0.013	0.141	0.982	$\approx 10^{-4}$	0.139	1.11	0.982
Rydberg	future	60	0.5	0.4	0.99	$\approx 10^{-4}$	≈ 0.4	120	0.99

TABLE S4. Table comparing the performances of different atomic single-photon sources. Here \mathcal{R} is weighted by the duty cycle of operation. Values estimated from available data.

[S1] S. Rosi, A. Burchianti, S. Conclave, D. S. Naik, G. Roati, C. Fort, and F. Minardi, “ λ -enhanced grey molasses on the d_2 transition of rubidium-87 atoms,” Scientific reports **8**, 1301 (2018).

- [S2] S. de Léséleuc, D. Barredo, V. Lienhard, A. Browaeys, and T. Lahaye, “Analysis of imperfections in the coherent optical excitation of single atoms to rydberg states,” *Phys. Rev. A* **97**, 053803 (2018).
- [S3] N. Šibalić, J. D. Pritchard, C. S. Adams, and K. J. Weatherill, “Arc: An open-source library for calculating properties of alkali rydberg atoms,” *Computer Physics Communications* **220**, 319–331 (2017).
- [S4] M. Saffman and T. G. Walker, “Creating single-atom and single-photon sources from entangled atomic ensembles,” *Phys. Rev. A* **66**, 065403 (2002).
- [S5] M. J. Stevens, “Photon Statistics, Measurements, and Measurements Tools,” in *Experimental Methods in the Physical Sciences*, (Elsevier, 2013), pp. 25–52.
- [S6] R. Uppu, T. A. Wolterink, T. B. Trentup, and P. W. Pinkse, “Quantum optics of lossy asymmetric beam splitters,” *Optics express* **24**, 16440–16449 (2016).
- [S7] J. R. Johansson, P. D. Nation, and F. Nori, “Qutip 2: A python framework for the dynamics of open quantum systems,” *Computer Physics Communications* **184**, 1234–1240 (2013).
- [S8] A. V. Gorshkov, A. André, M. D. Lukin, and A. S. Sørensen, “Photon storage in Λ -type optically dense atomic media. ii. free-space model,” *Phys. Rev. A* **76**, 033805 (2007).
- [S9] X.-L. Wang, L.-K. Chen, W. Li, H.-L. Huang, C. Liu, C. Chen, Y.-H. Luo, Z.-E. Su, D. Wu, Z.-D. Li, H. Lu, Y. Hu, X. Jiang, C.-Z. Peng, L. Li, N.-L. Liu, Y.-A. Chen, C.-Y. Lu, and J.-W. Pan, “Experimental ten-photon entanglement,” *Phys. Rev. Lett.* **117**, 210502 (2016).
- [S10] C. Xiong, X. Zhang, Z. Liu, M. J. Collins, A. Mahendra, L. Helt, M. J. Steel, D.-Y. Choi, C. Chae, P. Leong *et al.*, “Active temporal multiplexing of indistinguishable heralded single photons,” *Nat Commun* **7**, 10853 (2016).
- [S11] F. Kaneda and P. G. Kwiat, “High-efficiency single-photon generation via large-scale active time multiplexing,” *Science Advances* **5**, eaaw8586 (2019).
- [S12] N. Somaschi, V. Giesz, L. De Santis, J. Loredo, M. P. Almeida, G. Hornecker, S. L. Portalupi, T. Grange, C. Antón, J. Demory *et al.*, “Near-optimal single-photon sources in the solid state,” *Nature Photon* **10**, 340–345 (2016).
- [S13] J. C. Loredo, N. A. Zakaria, N. Somaschi, C. Anton, L. de Santis, V. Giesz, T. Grange, M. A. Broome, O. Gazzano, G. Coppola, I. Sagnes, A. Lemaitre, A. Auffeves, P. Senellart, M. P. Almeida, and A. G. White, “Scalable performance in solid-state single-photon sources,” *Optica* **3**, 433–440 (2016).
- [S14] H. Wang, Y. He, Y.-H. Li, Z.-E. Su, B. Li, H.-L. Huang, X. Ding, M.-C. Chen, C. Liu, J. Qin *et al.*, “High-efficiency multiphoton boson sampling,” *Nature Photon* **11**, 361–365 (2017).
- [S15] G. Kiršanskė, H. Thyrrerstrup, R. S. Daveau, C. L. Dreeßen, T. Pregolato, L. Midolo, P. Tighineanu, A. Javadi, S. Stobbe, R. Schott, A. Ludwig, A. D. Wieck, S. I. Park, J. D. Song, A. V. Kuhlmann, I. Söllner, M. C. Löbl, R. J. Warburton, and P. Lodahl, “Indistinguishable and efficient single photons from a quantum dot in a planar nanobeam waveguide,” *Phys. Rev. B* **96**, 165306 (2017).
- [S16] H. Wang, Y.-M. He, T.-H. Chung, H. Hu, Y. Yu, S. Chen, X. Ding, M.-C. Chen, J. Qin, X. Yang *et al.*, “Towards optimal single-photon sources from polarized microcavities,” *Nature Photon* **13**, 770–775 (2019).
- [S17] P. Maunz, D. Moehring, S. Olmschenk, K. Younge, D. Matsukevich, and C. Monroe, “Quantum interference of photon pairs from two remote trapped atomic ions,” *Nature Phys* **3**, 538–541 (2007).
- [S18] W. Rosenfeld, D. Burchardt, R. Garthoff, K. Redeker, N. Ortegel, M. Rau, and H. Weinfurter, “Event-ready bell test using entangled atoms simultaneously closing detection and locality loopholes,” *Phys. Rev. Lett.* **119**, 010402 (2017).
- [S19] J. K. Thompson, J. Simon, H. Loh, and V. Vuletić, “A high-brightness source of narrowband, identical-photon pairs,” *Science* **313**, 74–77 (2006).
- [S20] T. Wilk, S. C. Webster, H. P. Specht, G. Rempe, and A. Kuhn, “Polarization-controlled single photons,” *Phys. Rev. Lett.* **98**, 063601 (2007).
- [S21] P. B. R. Nisbet-Jones, J. Dille, D. Ljunggren, and A. Kuhn, “Highly efficient source for indistinguishable single photons of controlled shape,” *New Journal of Physics* **13**, 103036 (2011).
- [S22] M. Mücke, J. Bochmann, C. Hahn, A. Neuzner, C. Nölleke, A. Reiserer, G. Rempe, and S. Ritter, “Generation of single photons from an atom-cavity system,” *Phys. Rev. A* **87**, 063805 (2013).